Journal of Materials Chemistry C

Photomechanical Molecular Crystals and Nanowire Assemblies Based on the [2+2] Photodimerization of a Phenylbutadiene Derivative

Journal:	*Journal of Materials Chemistry C*
Manuscript ID	TC-ART-12-2019-006946.R1
Article Type:	Paper
Date Submitted by the Author:	05-Feb-2020
Complete List of Authors:	Tong, Fei; University of California at Riverside, Chemistry Xu, Wenwen; University of Massachusetts Amherst, Polymer Science and Engineering Guo, Tianyi; Kent State University, Advanced Materials and Liquid Crystal Institute Lui, Brandon; University of California Riverside, Hayward, Ryan; University of Massaschusetts, Polymer Science and Engineering Palffy-Muhoray, Peter; Kent State University, Advanced Materials and Liquid Crystal Institute Al-Kaysi, Rabih; King Saud bin Abdulaziz University for Health Sciences, Basic Sciences Bardeen, Christopher; University of California at Riverside, Chemistry

Photomechanical Molecular Crystals and Nanowire Assemblies Based on the [2+2] Photodimerization of a Phenylbutadiene Derivative

Fei Tong[(1)], Wenwen Xu[(2)], Tianyi Guo[(3)], Brandon F. Lui[(1)], Ryan C. Hayward[(2)], Peter Palffy-Muhoray[(3)], Rabih O. Al-Kaysi[(4)*], Christopher J. Bardeen[(1)(5)*]

(1) Chemistry Department
University of California, Riverside
Riverside, CA 92521 (USA)

(2) Department of Polymer Science and Engineering
University of Massachusetts Amherst
120 Governors Drive
Amherst, MA 01003 (USA)

(3) Advanced Materials and Liquid Crystal Institute
Kent State University
1425 University Esplanade
Kent, OH 44242 (USA)

(4) College of Science and Health Professions-3124,
King Saud bin Abdulaziz University for Health Sciences, and King Abdullah International Medical Research Center, Ministry of National Guard Health Affairs, Riyadh 11426,
(Kingdom of Saudi Arabia)

(5) Department of Materials Science & Engineering
University of California, Riverside
Riverside, CA 92521 (USA)

Emails of the corresponding authors: christopher.bardeen@ucr.edu, rabihalkaysi@gmail.com

Abstract

(*E*)-4-fluoro-cinnamaldehyde malononitrile ((*E*)-**4FCM**) is a new phenylbutadiene derivative that undergoes a [2+2] photocycloaddition in the crystal form. Optical absorption and proton nuclear magnetic resonance (^{1}H-NMR) measurements demonstrate that the solid-state (*E*)-**4FCM** photodimerization is a negative photochromic reaction that proceeds to 97% completion. The large geometry change and full conversion allow bulk crystals of (*E*)-**4FCM** to show strong photosalient effects when exposed to 405 nm ultraviolet light. When (*E*)-**4FCM** nanowires are grown in an anodic alumina oxide (AAO) template, they maintain a high degree of crystallinity and orientation, as determined by X-ray diffraction measurements. When illuminated, (*E*)-**4FCM** nanowire bundles exhibit a rapid expansion, during which they spread by as much as 300% in the lateral direction. This lateral expansion is at least partially due to a photoinduced crystal expansion along the diameter of the nanowires. When (*E*)-**4FCM** nanowires are confined inside the AAO template, the photoinduced expansion can be harnessed to deform the template, causing it to bend under UV light irradiation. The bending motion due to 2.0 mg of **4FCM** in a template can cause the template to bend by up to 1.0 mm and lift up to 200 g. These results represent a significant improvement in work output relative to previous composite actuator membranes based on diarylethene photochromes.

Introduction

Photomechanical molecular crystals are promising candidates for applications in actuators, switches, and waveguide devices.[1-4] Over the last decade, a number of photomechanical molecular crystals have been demonstrated that are powered by a variety of photochemical reactions and undergo a variety of photoinduced motions such as bending[5-15], twisting[16-18], rotation[19], crawling[20], peeling[21-22], and hopping[23]. In order to maximize the force generated by a photomechanical crystal, the photochemical reaction should proceed to completion. This can be challenging for reactions in which the photoproduct absorption overlaps that of the reactant. For example, photoreactions involving the *E*-*Z* photoisomerization of azobenzenes tend to reach an equilibrium photostationary state (PSS) whose absorption hinders further progress of the photoreaction and can prevent deeper light penetration into the sample.[24-26] In contrast, a molecule that undergoes a "negative" photochromic reaction, in which the photoproduct absorption shifts to higher energies, should permit the photoreaction to go to 100% completion even in a thick crystal.[27]

Our research group has focused on intermolecular [2+2] and [4+4] photocycloaddition reactions because they exhibit negative photochromism (which leads to high photochemical conversion) accompanied by large changes in molecular geometry (which leads to a large photomechanical response). For example, (*E*)-cinnamic acid undergoes a negative photochromic reaction based on a [2+2] photocycloaddition between neighboring molecules in specific crystal polymorphs.[28-31] While this reaction has been successfully harnessed to generate photomechanical crystals[32-38], molecules based on this structural motif tend to absorb in the ultraviolet (UV) around 300 nm or below. In order to push toward longer wavelengths,

we investigated derivatives with a 1,3-butadiene group attached to the core phenyl group. The additional vinyl should increase the electronic conjugation, extending the absorption into the near-UV and visible regions. Herein, we report the properties of one such derivative, (*E*)-4-fluoro-cinnamaldehyde malononitrile ((*E*)-**4FCM**). By itself in solution, (*E*)-**4FCM** undergoes an *E*→*Z* unimolecular photoisomerization, similar to other butadiene derivatives (Scheme 1a). But in the crystal form, it undergoes a [2+2] photodimerization (Scheme 1b) under 405 nm light irradiation. This negative photochromic reaction can approach complete conversion of the monomer to photodimer in the solid-state. (*E*)-**4FCM** bulk crystals and nanocrystals show very vigorous photomechanical behavior, involving photosalient effects and various types of mechanical motions (expanding, bending and curling). The large conversion and dramatic structural changes allow this material to generate substantial work, as measured by the photoinduced bending of a porous anodic aluminum oxide (AAO) template that incorporates crystalline (*E*)-**4FCM** nanowires. A few milligrams of material can generate enough work to displace up to 200 grams. Our results demonstrate a new class of photomechanical molecular crystals that can be incorporated into composite materials and generate a large amount of mechanical work.

Experimental

Materials and Methods

4-fluorocinnamaldehyde (> 95%, GC) was purchased from Tokyo Chemical Industry-America (TCI-America) and refigerated under argon. Piperidine (Reagent Plus, 99%) was purchased from Sigma-Aldrich and malononitrile (>98%, GC) was purchased from UFC-biotechnology,

Riyadh, Saudi Arabia. Both dichloromethane and acetonitrile were distilled over CaH_2 and stored over activated molecular sieves (3Å). Millipore water (15 ohm) was used for all experiments. All solvents and reagents were of reagent grade (Sigma-Aldrich) and were used as received. Commercial anodic aluminum oxide (AAO) templates (Whatman Anodisc, diameter 13 mm, average pore diameter 0.2 μm) were purchased from Sigma-Aldrich.

Samples were mixed with infrared (IR) grade KBr using an Agate mortar and pestle, then pressed into transparent pellets for IR spectroscopy measurements. A JNM-ECS 400 spectrometer (JEOL) and an Avance NEO 400 (Bruker) were used for NMR measurements. High Performance Liquid Chromatography (HPLC) analysis was performed on a Shimadzu (LC-20AD) using a Thermo Scientific general purpose BDS Hypersil C18 column (250 × 4.6 mm) held at a constant temperature of 35ºC. A gradient mobile phase was used starting with 50% aqueous acetonitrile in water (pH = 2.5) finishing with 100% acetonitrile at a flow rate of 1.5 mL/min.

Synthesis of 2-[3-(4-fluoro-phenyl)-allylidene]-malononitrile, (*E*)-4FCM

Briefly, 4-fluorocinnamaldehyde (1.0 g, 0.0067 moles), malononitrile (0.88 g, 0.013 moles) and dichloromethane (25 mL) were added into a 50 mL round bottom flask. The mixture was stirred at room temperature under an argon atmosphere until the reactants dissolved. Crushed activated molecular sieves (3Å) were added to the solution, followed by piperidine (0.05 mL) as the catalyst. The reaction was stirred at room temperature for 3-4 hours until the aldehyde was consumed. The reaction progress was monitored using silica thin-layer chromatrography

with 75% hexanes/ 25% ethyl acetate mobile phase. The dark yellow reaction mixture was filtered through an activated basic alumina plug to remove residual water and unreacted malononitrile. The dichloromethane was removed under reduced pressure to yield a crude yellow solid, which was recrystallized from boiling methanol/water (V/V=1:1). Yellow crystals were obtained after recrystallization (>99%, HPLC, yield 58%). M.P. = 143-144 ^{o}C. Infrared spectroscopy (IR) measurements were performed on an IR Affinity-1 FT-IR from Shimadzu. The IR spectrum is given in Fig.S1 (ESI). ^{1}H-NMR (400 MHz, DMSO-d_6): δ (ppm) = 7.22-7.28 (1H, dd, J = 16, 12 Hz), 7.30-7.35 (2H, ddd, J = 8, 4 Hz), 7.58-7.62 (1H, d, J = 16 Hz), 7.87-7.90 (2H, ddd, J = 8, 4 Hz), 8.26-8.29 (1H, d, J = 12 Hz). ^{13}C-NMR (100 MHz, DMSO-d_6): δ = 163.32-165.81 (J = 249.8 Hz), 132.30-132.39, 150.38, 162.65 (J = 8.6 Hz), 131.40-131.43, 123.04-123.06 (J = 1.9 Hz), 116.84-117.06 (J = 21.9 Hz), 81.42, 112.74, 114.75 (Fig. S2 and S3, ESI).

Solid-state photochemical synthesis of the (*E*)-4FCM photodimer

(*E*)-**4FCM** crystals (50 mg) were placed inside a Schlenk flask (50 mL) with deionized water (20 mL). The yellow (*E*)-**4FCM** crystals aggregated and floated on top of the water but could be suspended using a combination of agitation and sonication under argon gas. The tube was placed in the center of a light-emitting diode array which emitted light ranging from 410-500 nm with maximum intensity at 455 nm. The yellow suspension was stirred for several hours until it became white. The photoproduct was obtained after suction filtration and air-drying. The IR spectrum is given in Fig. S4 (ESI) ^{1}H-NMR (400 MHz, acetone-d_6): δ (ppm) = 7.82-7.85 (2 H, d, J = 9.6 Hz), 7.57-7.60 (4H, dd, J = 8 Hz, 4 Hz), 7.20-7.24 (4H, t, J = 8.8 Hz),

4.58-4.67 (4H, m). ^{13}C-NMR (100 MHz, acetone-d_6): δ = 160.99-163.43, 168.88 (J = 244 Hz), 133.32-133.36 (J = 4 Hz), 129.83-129.91 (J = 8 Hz), 115.63-115.85 (J = 22 Hz), 44.69, 45.65, 89.43, 110.96, 112.17 (Fig. S5 and S6, ESI).

Preparation of (*E*)-4FCM nanowires

A concentrated solution of (*E*)-**4FCM** was prepared by dissolving roughly 6.5 mg in N, N-DMF (60 μL). The solution was deposited on an AAO template. The AAO template was then suspended on top of a hollow glass holder (3 cm in height). The entire setup was covered with a glass bell jar and placed inside a convection oven set at 65ºC for a period of 48 h. The N, N-DMF solvent evaporated slowly from the bell jar, leaving the crystallized (*E*)-**4FCM** inside and on the surface of the AAO template. The loaded AAO template was then carefully polished with 2000 grit sandpaper to remove surface crystals. To isolate individual nanowires and bundles, the template was dissolved in a H_3PO_4/SDS (wt:20%/0.1%) aqueous solution.

X-ray diffraction measurements

To determine the molecular orientation of (*E*)-**4FCM** nanowires inside the AAO templates, we employed grazing incidence wide-angle X-ray scattering (GI-WAXS). All the GI-WAXS data were collected by a Ganesha SAXS-LAB instrument at room temperature. The X-ray wavelength is 0.154 nm (CuK_α radiation). (*E*)-**4FCM** filled AAO templates were cut into small pieces (1 mm × 3 mm) and mounted on a manual mini rotation Stage (Thorlabs, MSRP01). The incident angle is defined as the angle between the X-ray beam and the AAO surface and was fixed at 2° from the AAO membrane surface. This angle is well above the critical angle,

so the X-rays probe the bulk of the sample. WAXS patterns were recorded by a 2D detector (Pilatus 300K).

Optical spectroscopy measurements

All UV-Vis absorption spectra were obtained using a Varian CARY 60 spectrometer. Solid-state polycrystalline thin films were prepared by depositing about 100 μL of a 0.05 M **4FCM** methylene chloride solution onto a clean glass microscope slide and allowing the solvent to evaporate.

Optical microscopy measurements

For (*E*)-**4FCM** bulk crystals, several milligrams of the (*E*)-**4FCM** powders were deposited onto a glass slide. A coverslip was placed on top in order to prevent the crystals from jumping off the glass slide during irradiation. For the nanowire measurements, 1-2 drops of the (*E*)-**4FCM** nanowire suspension were deposited onto a glass slide. A coverslip was placed on top in order to reduce the rate of water evaporation. To monitor the photomechanical motions, an Olympus IX70 microscope (equipped with an AMScope MU900 digital camera) and Leica DM2700 M microscope (equipped with a Leica MC120 HD digital camera) were used. (*E*)-**4FCM** samples were irradiated using either 365 nm or 405 nm light from the fluorescence microscope Hg lamp (100 W), filtered through a dichroic mirror. For cross-polarized optical microscopy measurements, the sample was placed between two square (4 cm × 4 cm) polarizers aligned at 90° angle with respect to each other.

Scanning Electron Microscopy (SEM) measurements

A few drops of (*E*)-**4FCM** nanowires suspension were deposited on an AAO template, rinsed with plenty of Milli-Q purified water, and dried by vacuum filtration. After further drying in an oven at 65ºC for 24 h, the AAO template was stuck to a piece of conducting copper tape that was then fixed on a SEM stub. The SEM stubs were placed in a sputter coater (Cressington 108 Auto) and coated with Pt/Pd for 45 seconds to improve the sample conductivity. The SEM (FEI NNS450) imaged the sample using a 20 kV electron beam in high vacuum (10^{-7}) torr and an Everhart-Thornley Detector.

Results and Discussion

In methanol solution, (*E*)-**4FCM** shows an absorption band at 347 nm associated with $S_0 \rightarrow S_1$ transition and a smaller peak at around 250 nm that corresponds to the $S_0 \rightarrow S_2$ transition. The peak at 347 nm is redshifted by ~80 nm as compared to the longest wavelength absorption of cinnamic acid, as expected for increased intramolecular π-conjugation across the divinyl group.[39] (*E*)-**4FCM** undergoes an E→Z photoisomerization under UV light irradiation (365 nm, intensity~2.5mW/cm^2) as evidenced by the absorbance decrease of about 35% after 3 min light irradiation. The absorbance maximum shifts blue by about 5 nm, and there is an isosbestic point at around 305 nm (Fig. 1a), indicating a single photoisomer is formed, presumably after *E-Z* isomerization around one of the double bonds.[40] Continued illumination lead to no further changes, indicating that a photostationary state (PSS) has been attained. At these concentrations, there is no sign of photodimer formation in solution.

The UV-Vis absorption spectrum of a (*E*)-**4FCM** polycrystalline thin film shows a broad

absorbance extending out to 420 nm (Fig. 1b). Presumably the redshift is caused by the higher dielectric constant and intermolecular interactions in the solid. The solid-state (*E*)-**4FCM** photochemistry exhibits a very different trend from that in the liquid phase, with a steady decline under UV light irradiation (405nm, intensity ~8 mW/cm^2). After 1.5 hours of UV illumination, the absorbance drops by about 90%, and the film turns from yellow to pale white (Fig. S7, ESI). The loss of absorbance during light irradiation, i.e. negative photochromism, is not consistent with *E*-*Z* photoisomerization. After the fully photoreacted solid-state sample was dissolved in deuterated acetone, NMR was used to assess the reaction products. The ^{1}H-NMR measurements show the appearance of a cyclobutane multiplet at 4.4 ppm, signaling the dimerization of (*E*)-**4FCM** (Fig. 1c and 1d).[41-42] The complete disappearance of the vinyl protons at around 7.6 and 7.2 ppm shows that ~97% of the starting material has been consumed. No signatures of the *Z* isomer could be detected, implying that the monomer is converted only to dimer. This dimerization occurs exclusively across the first double bond, since the vinyl proton signals of this bond at 7.6 and 7.2 ppm completely disappears, while the other vinyl proton signal at 8.3 ppm shifts to 8.0 ppm but does not lose intensity.

Based on the crystal structure, the photodimerization of (*E*)-**4FCM** monomers is expected because the distance between two monomer pairs is about 3.376 Å (< 4.2 Å) and allows dimerization according to the Schmidt topochemical principle (Fig. 2a and table S1, ESI). [43-45] The solid-state photodimerization of a different phenylbutadiene derivative that adopts a similar head-to-tail packing arrangement has been previously reported.[46-47] The resulting photodimer is thermally stable and can be crystallized from 1-propanol. The crystal structure of the recrystallized photodimer is shown in Fig. 2c and 2d. As expected from the NMR

analysis, only the first double bond participates in the [2+2] photocycloaddition. As shown in Fig. 2, the photodimer adopts a butterfly-like geometry as the cyclobutane C-C bond decreases the center-to-center distance from 3.376 Å to 1.586 Å, while the distance between the outer edges (from the F atom one phenyl group to the N atom on the opposing cyano group) elongates from 4.281 Å to 5.995 Å (Fig. 2a and 2c). The huge distortion in geometry causes a molecular volume increase from 486.992 $Å^3$ for the monomer pair to 501.615 $Å^3$ for the photodimer (ΔV = 14.623 $Å^3$, ESI).

The substantial geometry change that accompanies the solid-state photodimerization, along with its very high yield, motivated us to study the photomechanical behavior of (*E*)-**4FCM** crystals. Under 405 nm light, (*E*)-**4FCM** bulk crystals exhibit very robust photosalient behavior including splitting, hopping and exploding (Fig. S8 and Movie S1, ESI). The crystals tend to shatter and fall apart during irradiation and the fragments appear to expand by about 5~15% after prolonged irradiation (Fig. S9 and S10, ESI).

The strong photomechanical behavior in (*E*)-**4FCM** bulk crystals was preserved when crystal dimensions were shrunk down to the nanoscale. The benefit of decreasing the crystal size is that smaller crystals are more capable of surviving photochemical transformations without fracturing. We succeeded in growing nanowires of (*E*)-**4FCM** by slow solvent annealing in anodic aluminum oxide (AAO) templates.

To determine the orientation of (*E*)-**4FCM** nanowire crystals within the AAO templates, we performed grazing incidence wide-angle X-ray scattering (GI-WAXS), as outlined in Fig. 3. The resultant 2D WAXS pattern (Fig. 3b) shows reflections both along and out of the film plane, which is indicated by a white line and is tilted approximately 4° from vertical due to the

slight curvature of the AAO template. Both the (100) and (10-1) Miller planes (as well as their inverses (-100) and (-101)) show intense diffract spots along this direction. This observation indicates that these planes lie parallel to the surface normal and thus the crystallographic *b* axis is parallel to the nanowire axis, since this axis is parallel to both (100) and (10-1) planes (Fig. 3c). Further support for this assignment is provided by the locations of the (11-1) and (02-2) planes, which agree well with their calculated positions in Table 1. The details of the calculations are provided in the ESI. The narrow widths of the diffraction arcs (full-widths-at-half-maximum of 3.5°– 4.5°, Fig. S11) along the azimuthal direction in Fig. 3b indicate a high degree of crystal alignment relative to the surface normal and the molecular orientations inside (*E*)-**4FCM** nanowires are shown in Fig. 3d. On the other hand, the appearance of multiple well-resolved peaks in a single GI-WAXS pattern indicates that the individual nanowires can take on different orientations around the normal to the membrane surface. Both observations are consistent with vertically oriented nanowires inside the template that have random rotations along the normal axis. Further analysis of the GI-WAXS pattern is complicated by the presence of diffraction spots from the (*E*)-**4FCM** dimer crystal even before intentionally exposing to UV light, presumably due to exposure from ambient sources during fabrication and handling.

After dissolving the AAO template, an aqueous suspension of crystalline nanowires of (*E*)-**4FCM** could be harvested as shown in Fig. 4a. Under weak UV light irradiation (405 nm, intensity~ 4 mW/cm^2), individual (*E*)-**4FCM** nanowires gradually deformed with an elongation of the long axis by about 4 % (Fig. 4b). After extended illumination, the nanowires coiled up (Fig.4c-d, Fig. S12-S13 and movie S2, ESI) in a manner similar to that of dimethyl-2(3-

anthracen-9-yl)allylidene)malonate nanowires that undergo a crystal-to-amorphous transition.[48-49] Bundles of (*E*)-**4FCM** nanowires showed an explosive expansion within 1 second (Fig. S14 and Movie S3, ESI) under intense UV irradiation (400mW/cm^2). This rapid expansion could be slowed by lowering the intensity of the light to allow the strain to be released more gently. Fig. 5 and Movie S4 show the dynamics of a bundle at an intensity of ~40mW/cm^2, where the nanowire bundle spreads like an accordion. This spreading reflects the deformation of thousands of individual nanowires, with a lateral increase of more than 300% of the original length. When even lower intensities were used, the bundles still spread out, but more slowly. The fact that the same endpoint could be reached with different light intensities argues against photothermal effects, because in that scenario spreading would only be observed for high heating at high intensities.

The photoinduced deformation of the nanowires is driven at least in part by a crystal-to-crystal expansion along their short axis. This expansion is too small to be observed by optical microscopy but could be discerned by SEM imaging of the nanowires before and after UV exposure. Care was taken to limit the duration of the exposure to a period that was shorter than that required to generate the amorphous phase. The images in Fig. 6 and Fig. S15 show that there is an increase in the average diameter from 234.7 ± 20.9 nm to 278.4 ± 38.2 nm. This ~15% increase in average diameter must be associated with an expanded crystal lattice when the photodimer is present. After longer periods of irradiation, nanowires in suspension lose their crystallinity as observed through the disappearance of the birefringence under a cross-polarized microscope (Fig. S16, ESI). The photodimer crystals inside the AAO template also become largely amorphous eventually after prolonged light irradiation, as judged by the

progressive weakening of diffraction peaks in the GI-WAXS patterns (Fig S17, ESI).

Previously, our group demonstrated that a hybrid organic-inorganic composite with diarylethene (**DAE**) nanowires inside an AAO template could function as a photoactuator and lift macroscopic objects.[50-51] The AAO template aligns the nanowires while providing structural support and a high elastic modulus. To see whether the large expansion of the (*E*)-**4FCM** nanowires along their diameter could produce useful mechanical work, we clamped an AAO template containing (*E*)-**4FCM** nanowires between two opaque glass slides and irradiated it from the bottom. Without any load, the template could bend away from the light source by almost 1 mm (0.92 mm) with a bending curvature as large as 13 m^{-1} (Fig. S18 and Movie S5, ESI). The curvature was maintained after the excitation light was switched off. After bending, continued light exposure resulted in extrusion of the **4FCM** from the bottom of the template on the same timescale that the crystal-to-amorphous transition we measured by PXRD (Fig. S19). A 1.28 g mirror on top of an (*E*)-**4FCM**/AAO template could be elevated by about 0.26 mm by this bending motion (Fig. 7). We found that the bending template could lift as much as 200 g, or roughly 2×10^5 times its own weight, by about 1.5 ~ 2 μm (Fig. S20 and Movie S6). This mass corresponds to a stopping force of 0.2 N, about 5× that seen for the **DAE**/AAO templates studied previously.[50] After exposure to UV, the template retains its bent shape for at least several hours (the image in Figure 7c was taken 2 hours after exposure) but over the course of several days the bend relaxes slightly.

Preliminary force-displacement measurements were also consistent with a larger work output. However, **4FCM**'s lack of reversibility prevented us from making repeated measurements on the same template. Although **4FCM** lacks the reversibility of the **DAE**

system, these results show that using a different photochromic reaction can substantially increase the work output. We attribute this increase in work output to the dramatic size increase of the nanowires inside the nano-channels of AAO template, coupled with the high conversion due to the negative photochromic reaction in the solid (*E*)-**4FCM**.

We hypothesize that the origin of the photoinduced bending of the **4FCM**/AAO template is similar to that of the **DAE**/AAO template. Considering the nanowire bundles as an assembly of loosely packed nanowires, under UV light irradiation the nanowires expand and deform, which then causes rapid separation of the assembly. However, when these nanowires are confined inside the channels of the AAO template, the channel walls in the AAO experience a lateral force from the nanowire expansion. The asymmetric expansion of the bottom of the template forms causes the bending. Even though this bending can generate more force than the **DAE** used in previous work, it is unlikely that we extract the full amount of mechanical energy associated with the nanowire expansion. First, we suspect that most of the photogenerated force is consumed in doing mechanical work against the high elastic modulus AAO template. Second, it appears that the photodimer crystal itself is not stable in the nanowire geometry. The transformation of the product to an amorphous phase during photoreaction is expected to reduce the work output, since the amorphous phase likely has a lower elastic modulus and is less effective in transmitting work to the channel walls. The observation that the photoproduct is extruded from the template during reaction is consistent with the idea that expanding amorphous material does not exert much lateral force, but instead deforms itself due to the physical confinement of the AAO pores. Based on these observations, improved performance might be achieved by finding a negative photochromic material that remains fully

crystalline throughout the photoreaction.

Conclusion

In conclusion, we have made a new molecular crystal, (*E*)-**4FCM** based on a phenylbutadiene framework that undergoes a negative photochromic [2+2] cycloaddition reaction. The large geometry changes that accompany the photodimerization reaction, along with the negative photochromic reaction that propels the photochemistry to nearly 97% completion, lead to a strong photomechanical response. Bulk crystals of (*E*)-**4FCM** show strong photosalient effects, including splitting, hopping, and fracture under light irradiation. Crystalline nanowires of (*E*)-**4FCM** prepared by the slow solvent annealing method can exhibit photoinduced bending and curling motions, while nanowire bundles show explosive expansions under intense UV light irradiation. When aligned inside an AAO template, the photomechanical effects of nanowires can be combined to generate forces large enough to bend the template while lifting up to 200 g. Although not reversible, the enhanced work and force generation of this new crystal relative to **DAE** demonstrate how the tools of organic chemistry can be used to prepare new photomechanical molecular crystals with enhanced performance.

Corresponding Authors

Email: christopher.bardeen@ucr.edu (C.J.B)

rabihalkaysi@gmail.com (R.O.K.)

ORCID

Fei Tong: 0000-0003-4545-2230

Brand F. Lui: 0000-0002-9765-4419

Ryan C. Hayward: 0000-0001-6483-2267

Rabih O. Al-Kaysi: 0000-0001-8429-2802

Christopher J. Bardeen: 0000-0002-5755-9476

Notes

The authors declare no competing financial interest.

Acknowledgments

This research was supported by the National Science Foundation grant DMR-1810514 and by the MURI on Photomechanical Material Systems (ONR N00014-18-1-2624). R.O.K. acknowledges the support of KSAU-HS/KSIMRC through grant RC10/104.

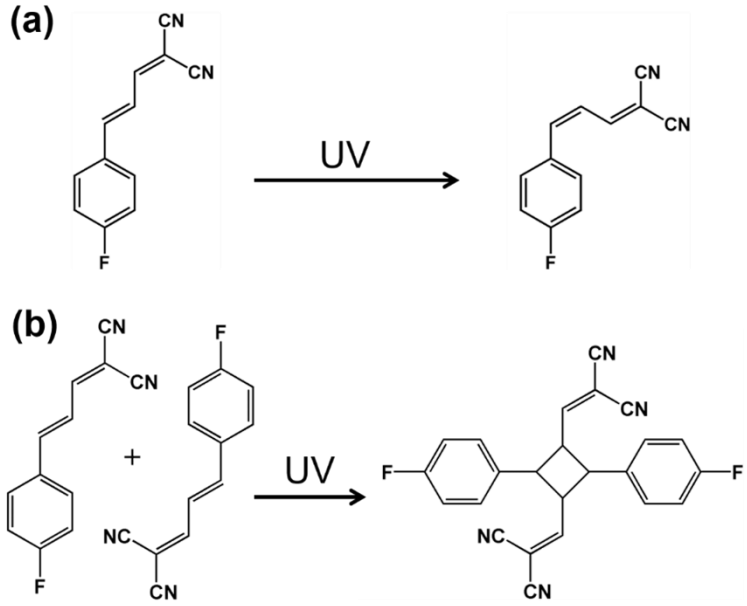

Scheme 1. (a) (*E*)-**4FCM** undergoes *E* to *Z* photoisomerization in liquid phase under UV light irradiation and (b) [2+2] photocycloaddition of solid-state (*E*)-**4FCM** to form the photodimer under UV light irradiation.

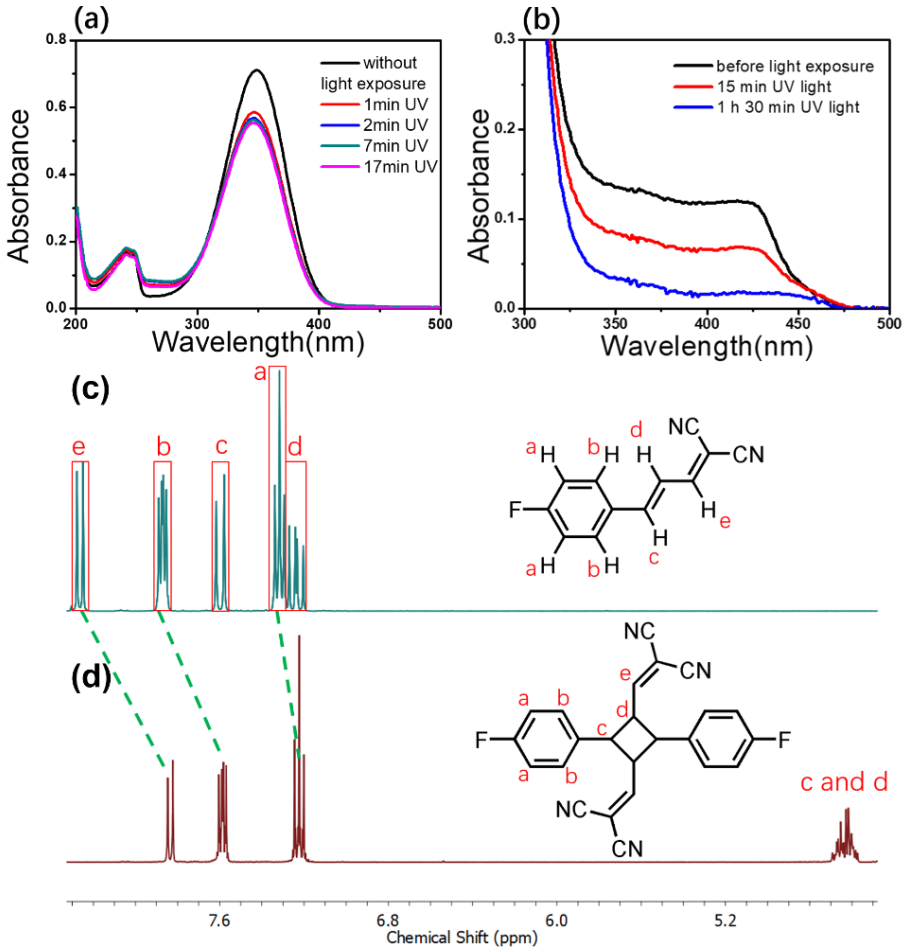

Fig. 1. (a) UV-Vis absorption of liquid phase sample in methanol before (black traces) and after UV light irradiation. The concentration of the sample is 3.8×10^{-5} M. (b) UV-Vis absorption of the solid-state polycrystalline thin film of a sample before (black traces) and after UV light irradiation (red and blue traces). The residual absorbance in the blue trace is due to remaining **4FCM** monomer in the thick, scattering film. (c) ^{1}HNMR spectrum of (*E*)-**4FCM** and (d) ^{1}HNMR spectrum of the (*E*)-**4FCM** photodimer, showing changes in aromatic and vinyl peaks.

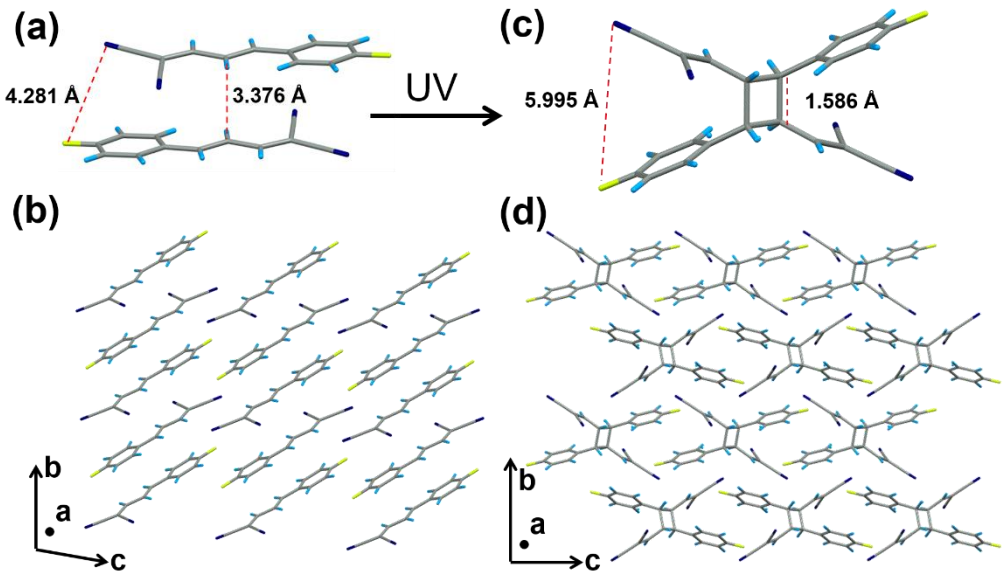

Fig. 2. (a) Crystal packing of monomer pairs of (*E*)-**4FCM**. (b) Crystal packing of (*E*)-**4FCM** monomer viewed along the *a* axis. (c) Molecular structure of **4FCM** photodimer and (d) Crystal packing of **4FCM** photodimer viewed along the *a* axis.

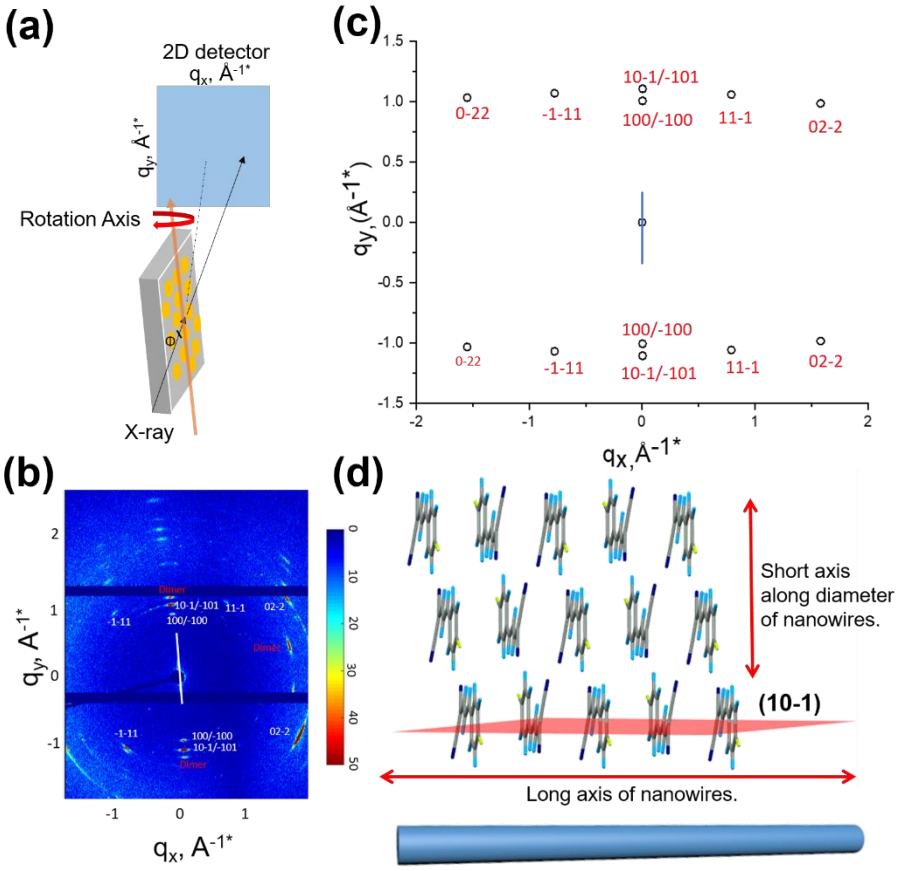

Fig.3. (a) Schematic illustration of GI-WAXS experimental geometry; the incident angle of the X-rays was Φ = 2°. (b) The resultant 2D WAXS pattern, with the AAO template plane indicated by a white line. The color map shows the relative intensity of X-rays. (c) The calculated locations of diffraction spots taking the *b* axis as the surface normal direction and allowing crystals to take on all possible transverse orientations. The AAO template plane is indicated by a blue line. (d) (*E*)-**4FCM** molecular orientation inside the nanowires. The (10-1) Miller plane is parallel to long axis of nanowires.

Table 1. Comparison of experimental and calculated angles between film plane and crystallographic reflections when *b* axis is oriented along the nanowire axes.

	(100)	(10-1)	(11-1)	(02-2)
Experimental	1.5°	1.9°	36.3°	58.8°
b axis as surface normal	0.3°	0.3°	36.8°	58.1°

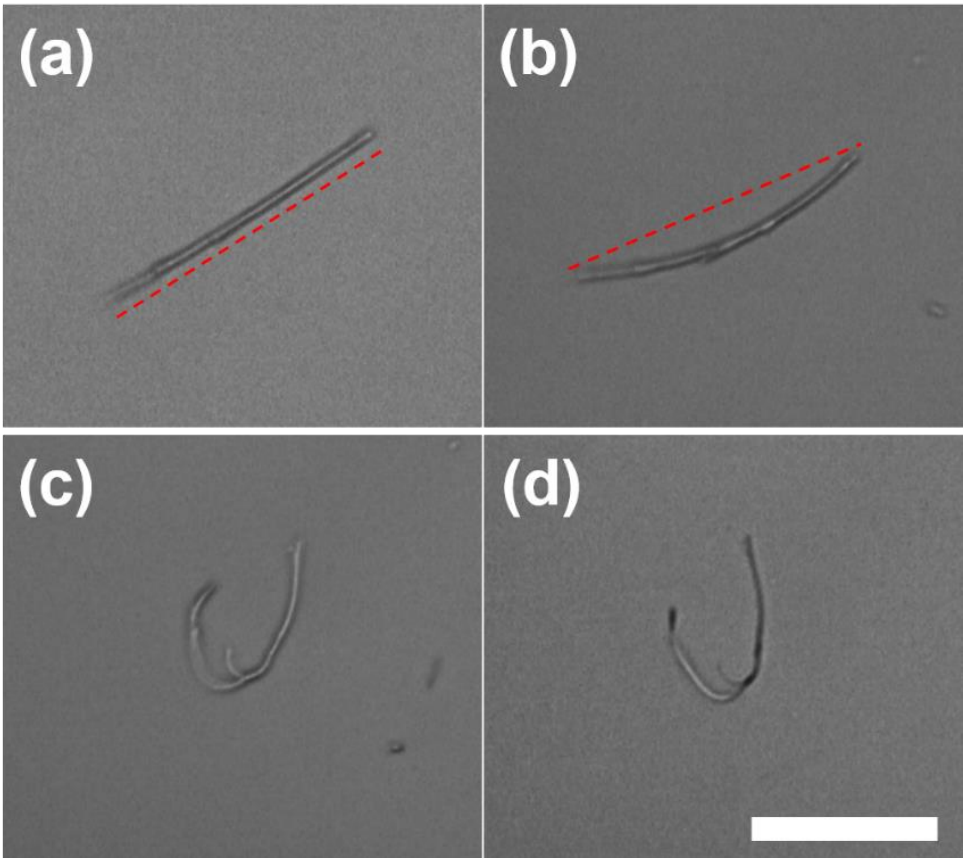

Fig. 4. (a)-(d) Sequential optical microscope images displaying photoinduced curling motion of an individual (*E*)-**4FCM** nanowire under weak UV light irradiation. The red dashed line shows the original length of the nanowire. Scale bar: 30 μm.

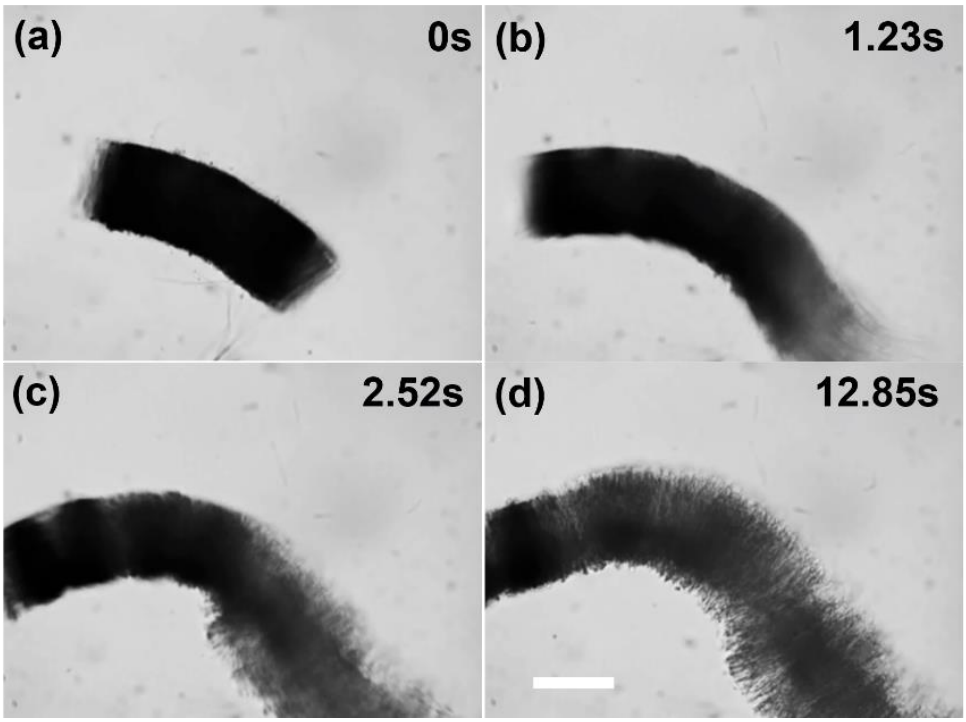

Fig. 5. Optical microscope images of a (*E*)-**4FCM** nanowire bundle spreading under UV light irradiation. The time shows the irradiation duration. White scale bar: 50μm.

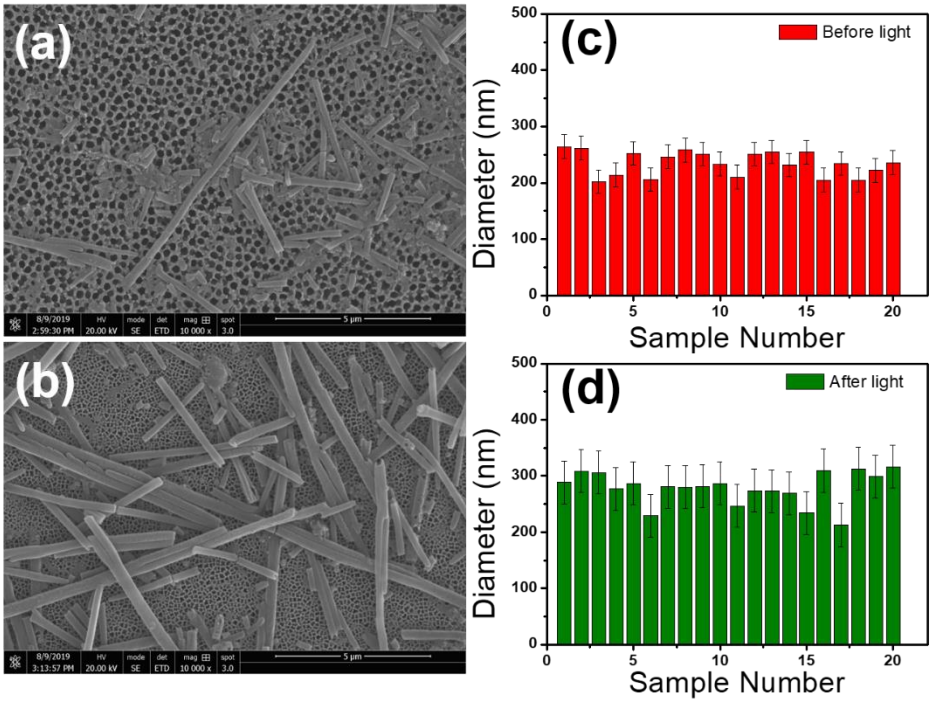

Fig. 6. (a) and (b) SEM images of **4FCM** nanowires harvested from the same AAO template before and after full light irradiation. Scale bar: 5 μm. (c) and (d) associated histograms of diameters of **4FCM** nanowires before and after full light irradiation.

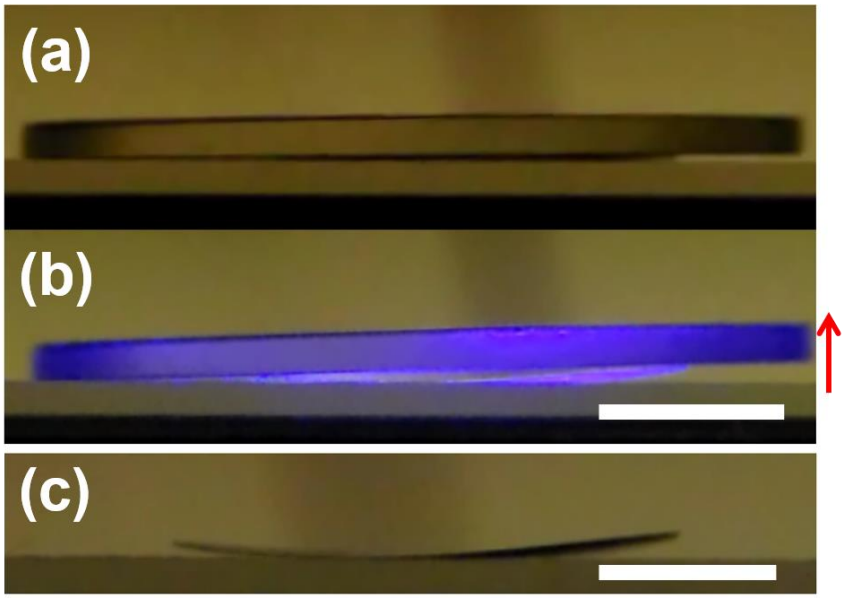

Fig. 7. Snapshots of **4FCM**/AAO template lifting a mirror (mass=1.28 g) under UV light irradiation from below. (a) before light and (b) 1s before the UV light switched off. (c) **4FCM**/AAO template curvature after the mirror is removed. The left half of the template has been masked to prevent photoreaction. The red arrow indicates the elevation direction of the mirror; scale bars = 5 mm.

References

(1) Garcia-Garibay, M. A., Molecular crystals on the move: From single-crystal-to-single-crystal photoreactions to molecular machinery. *Angew. Chem. Int. Ed.* **2007,** *46*, 2-5.

(2) Kim, T.; Zhu, L.; Al-Kaysi, R. O.; Bardeen, C. J., Organic Photomechanical Materials. *ChemPhysChem* **2014,** *15*, 400-414.

(3) Naumov, P.; Chizhik, S.; Panda, M. K.; Nath, N. K.; Boldyreva, E., Mechanically Responsive Molecular Crystals. *Chem. Rev.* **2015,** *115*, 12440-12490.

(4) White, T. J., *Photomechanical Materials, Composites, and Systems*. 1 ed.; Wiley: Hoboken, New Jersey, 2017.

(5) Al-Kaysi, R. O.; Bardeen, C. J., Reversible photoinduced shape changes of crystalline organic nanorods. *Adv. Mater.* **2007,** *19*, 1276-1280.

(6) Chizhik, S.; Sidelnikov, A.; Zakharov, B.; Naumov, P.; ab, E. B., Quantification of Photoinduced Bending of Dynamic Molecular Crystals: from Macroscopic Strain to Kinetic Constants and Activation Energies. *Chem. Sci.* **2018,** *9*, 2319–2335.

(7) Nath, N. K.; Pejov, L.; Nichols, S. M.; Hu, C.; Saleh, N.; Kahr, B.; Naumov, P., Model for photoinduced bending of slender molecular crystals. *J. Am. Chem. Soc.* **2014,** *136*, 2757-2766.

(8) Kobatake, S.; Takami, S.; Muto, H.; Ishikawa, T.; Irie, M., Rapid and reversible shape changes of molecular crystals on photoirradiation. *Nature* **2007,** *446*, 778-781.

(9) Morimoto, M.; Irie, M., A diarylethene cocrystal that converts light into mechanical work. *J. Am. Chem. Soc.* **2010,** *132*, 14172-14178.

(10) Kitagawa, D.; Tanaka, R.; Kobatake, S., Photoinduced Stepwise Bending Behavior of Photochromic Diarylethene Crystals. *CrystEngComm* **2016,** *18*, 7236-7240.

(11) Koshima, H.; Nakaya, H.; Uchimoto, H.; Ojima, N., Photomechanical motion of furylfulgide crystals. *Chem. Lett.* **2012,** *41*, 107-109.

(12) Koshima, H.; Ojima, N.; Uchimoto, H., Mechanical motion of azobenzene crystals upon photoirradiation. *J. Am. Chem. Soc.* **2009,** *131*, 6890-6891.

(13) Koshima, H.; Takechi, K.; Uchimoto, H.; Shiro, M.; Hashizume, D., Photmechanical bending of salicylideneaniline crystals. *Chem. Commun.* **2011,** *47*, 11423-11425.

(14) Bushuyev, O. S.; Tomberg, A.; Friscic, T.; Barrett, C. J., Shaping Cyrstals with Light: Crystal-to-Crystal Isomerization and Photomechanical Effect in Fluorinated Azobenzenes. *J. Am. Chem. Soc.* **2013,** *135*, 12556-12559.

(15) Samanta, R.; Ghosh, S.; Devarapalli, R.; Reddy, C. M., Visible Light Mediated Photopolymerization in Single Crystals: Photomechanical Bending and Thermomechanical Unbending. *Chem. Mater.* **2018,** *30*, 577−581.

(16) Zhu, L.; Al-Kaysi, R. O.; Bardeen, C. J., Reversible photoinduced twisting of molecular crystal microribbons. *J. Am. Chem. Soc.* **2011,** *133*, 12569-12575.

(17) Kitagawa, D.; Nishi, H.; Kobatake, S., Photoinduced twisting of a photochromic diarylethene crystal. *Angew. Chem. Int. Ed.* **2013,** *52*, 9320-9322.

(18) Kitagawa, D.; Tsujioka, H.; Tong, F.; Dong, X.; Bardeen, C. J.; Kobatake, S., Control of Photomechanical Crystal Twisting by Illumination Direction. *J. Am. Chem. Soc.* **2018,** *140*, 4208-4212.

(19) Zhu, L.; Al-Kaysi, R. O.; Bardeen, C. J., Photoinduced Ratchet-Like Rotational Motion of Branched Molecular Crystals. *Angew. Chem. Int. Ed.* **2016,** *55*, 7073-7076.

(20) Uchida, E.; Azumi, R.; Norikane, Y., Light-Induced Crawling of Crystals on a Glass Surface. *Nat. Commun.* **2015,** *6*, 7310/1-7.

(21) Tong, F.; Al-Haidar, M.; Zhu, L.; Al-Kaysi, R. O.; Bardeen, C. J., Photoinduced Peeling of Molecular Crystals. *Chem. Commun.* **2019,** *55*, 3709-3712.
(22) Cole, J. M.; Velazquez-Garcia, J. d. J.; Gosztola, D. J.; Wang, S. G.; Chen, Y.-S., Light-Induced Macroscopic Peeling of Single Crystal Driven by Photoisomeric Nano-Optical Switching. *Chem. Mater.* **2019,** *31*, 4927−4935.
(23) Naumov, P.; Sahoo, S. C.; Zakharov, B. A.; Boldyreva, E. V., Dynamic Single Crystals: Kinematic Analysis of Photoinduced Crystal Jumping (The Photosalient Effect). *Angew. Chem. Int. Ed.* **2013,** *52*, 9990 –9995.
(24) Durr, H.; Bouas-Laurent, H., *Photochromism : Molecules and Systems*. Elsevier: New York, 1990.
(25) Serra, F.; Terentjev, E. M., Nonlinear Dynamics of Absorption and Photobleaching of Dyes. *J. Chem. Phys.* **2008,** *128*, 224510/1-7.
(26) Shimamura, A.; Priimagi, A.; Mamiya, J.-i.; Ikeda, T.; Yu, Y.; Barrett, C. J.; Shishido, A., Simultaneous Analysis of Optical and Mechanical Properties of Cross-Linked Azobenzene-Containing Liquid-Crystalline Polymer Films. *ACS Appl. Mater. Interfaces* **2011,** *3*, 4190–4196.
(27) Aiken, S.; Edgar, R. J. L.; Gabbutt, C. D.; Heron, B. M.; Hobson, P. A., Negatively Photochromic Organic Compounds: Exploring the Dark Side. *Dyes Pigm.* **2018,** *149*, 92-121.
(28) Cohen, M. D.; Schmidt, G. M. J.; Sonntag, F. I., Topochemistry. Part II. The Photochemistry of trans-Cinnnamic Acids. *J. Chem. Soc.* **1964**, 2000-2013.
(29) Schmidt, G. M. J., Topochemistry. Part III. The Crystal Chemistry of Some trans-Cinnamic Acids. *J. Chem. Soc.* **1964**, 2014-2021.
(30) Friscic, T.; MacGillivray, L. R., Single-Crystal-to-Crystal [2+2] Photodimerization: from Discovery to Design. *Z. Kristallogr.* **2005,** *220*, 351-363.
(31) MacGillivray, L. R.; Papaefstathiou, G. S.; Friscic, T.; Hamilton, T. D.; Bucar, D. K.; Chu, Q.; Varshney, D. B.; Georgiev, I. G., Supramolecular control of reactivity in the solid state: from templates to ladderanes to metal-organic frameworks. *Acc. Chem. Res.* **2008,** *41*, 280-291.
(32) Naumov, P.; Kowalik, J.; Solntsev, K. M.; Baldridge, A.; Moon, J.-S.; Kranz, C.; Tolbert, L. M., Topochemistry and photomechanical effects in crystals of green fluorescent protein-like chromophores: effects of hydrogen bonding and crystal packing. *J. Am. Chem. Soc.* **2010,** *132*, 5845-5857.
(33) Kim, T.; Zhu, L.; Mueller, L. J.; Bardeen, C. J., Dependence of the solid-state photomechanical response of 4-chlorocinnamic acid on crystal shape and size. *CrystEngComm* **2012,** *14*, 7792-7799.
(34) Medishetty, R.; Husain, A.; Bai, Z.; Runceviski, T.; Dinnebier, R. E.; Naumov, P.; Vittal, J. J., Single crystals popping under UV light: a photosalient effect triggered by a [2+2] cycloaddition reaction. *Angew. Chem. Int. Ed.* **2014,** *53*, 5907-5911.
(35) Medishetty, R.; Sahoo, S. C.; Mulijanto, C. E.; Naumov, P.; Vittal, J. J., Photosalient Behavior of Photoreactive Crystals. *Chem. Mater.* **2015,** *27*, 1821-1829.
(36) Yadava, K.; Vittal, J. J., Photosalient Behavior of Photoreactive Zn(II) Complexes. *Cryst. Growth De.* **2019,** *19*, 2542-2547.
(37) Wang, H.; Chen, P.; Wu, Z.; Zhao, J.; Sun, J.; Lu, R., Bending, Curling, Rolling, and Salient Behavior of Molecular Crystals Driven by [2+2] Cycloaddition of a Styrylbenzoxazole Derivative. *Angew. Chem. Int. Ed.* **2017,** *56*, 9463 –9467.
(38) Shi, Y.-X.; Zhang, W.-H.; Abrahams, B. F.; Braunstein, P.; Lang, J.-P., Fabrication of Photoactuators: Macroscopic Photomechanical Responses of Metal–Organic Frameworks to Irradiation by UV Light. *Angew. Chem. Int. Ed.* **2019,** *58*, 9453 –9458.
(39) Zhu, L.; Tong, F.; Zaghloul, N.; Baz, O.; Bardeen, C. J.; Al-Kaysi, R. O., Characterization of a P-Type Photomechanical Molecular Crystal Based on the EàZ Photoisomerization of 9-Divinylanthracene Malonitrile. *J. Mater. Chem. C* **2016,** *4*, 8245-8452.

(40) Leslie R. Eastman, J.; Zarnegar, B. M.; Butler, J. M.; Whitten, D. G., An Unusual Case of Selectivity in a Photochemical Reaction. Photoisomerization of Unsymmetrical 1,3-Dienes. *J. Am. Chem. Soc.* **1974,** *96*, 2281-2283.

(41) Kole, G. K.; Kojima, T.; Kawano, M.; Vittal, J. J., Reversible Single-Crystal-to-Single-Crystal Photochemical Formation and Thermal Cleavage of a Cyclobutane Ring. *Angew. Chem. Int. Ed.* **2014,** *53*, 2143 – 2146.

(42) Panda, T.; Naumov, P., Time-Dependent Photodimerization of α-trans-Cinnamic Acid Studied by Photocalorimetry and NMR Spectroscopy. *Cryst. Growth Des.* **2018,** *18*, 2744−2749.

(43) Schmidt, G. M. J., Photodimerization in the Solid State. *Pure Appl. Chem.* **1971,** *27*, 647-678.

(44) Cohen, M. D., The Photochemistry of Organic Solids. *Angew. Chem. Int. Ed.* **1975,** *14*, 386-393.

(45) Ramamurthy, V.; Venkatesan, K., Photochemical Reactions of Organic Crystals. *Chem. Rev.* **1987,** *87*, 433-481.

(46) Row, T. N. C.; Swamy, H. R.; Acharyaa, K. R.; Ramamurthy, V.; Venkatesan, K.; Rao, C. N. R., Reversible Photodimerization of Phenylbutadienes in the Solid State. *Tet. Lett.* **1983**, 3263-3266.

(47) Swamy, H. R.; Ramamurthy, V.; Rao, C. N. R., Reversible Photodimerization of Some Butadiene Derivatives in Solid State. *Ind. J. Chem.* **1982,** *21B*, 79-82.

(48) Kim, T.; Al-Muhanna, M. K.; Al-Suwaidan, S. D.; Al-Kaysi, R. O.; Bardeen, C. J., Photoinduced Curling of Organic Molecular Crystal Nanowires. *Angew. Chem. Int. Ed.* **2013,** *125*, 7027-7031.

(49) Tong, F.; Liu, M.; Al-Kaysi, R. O.; Bardeen, C. J., Surfactant-Enhanced Photoisomerization and Photomechanical Response in Molecular Crystal Nanowires. *Langmuir* **2018,** *34*, 1627-1634.

(50) Dong, X.; Tong, F.; Hanson, K. M.; Al-Kaysi, R. O.; Kitagawa, D.; Kobatake, S.; Bardeen, C. J., Hybrid Organic−Inorganic Photon-Powered Actuators Based on Aligned Diarylethene Nanocrystals. *Chem. Mater.* **2019,** *31*, 1016−1022.

(51) Dong, X.; Guo, T.; Kitagawa, D.; Kobatake, S.; Palffy-Muhoray, P.; Bardeen, C. J., Effects of Template and Molecular Nanostructure on the Performance of Organic-Inorganic Photomechanical Actuator Membranes. *Adv. Funct. Mater.* **2019**, 1902396/1-9

Graphic Abstract

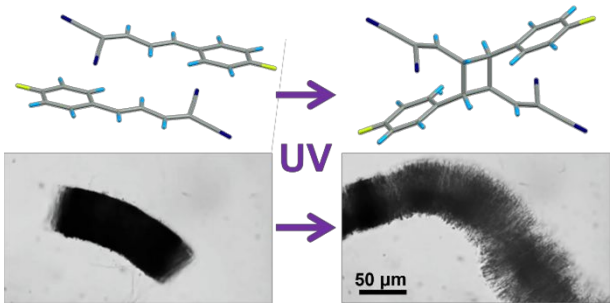

Crystalline (*E*)-4-fluoro-cinnamaldehyde malononitrile undergoes a [2+2] photocycloaddition, leading to a robust photomechanical response and improved force generation by nanowire ceramic composites.